Heliyon 10 (2024) e29984

Contents lists available at ScienceDirect

Heliyon

journal homepage: www.cell.com/heliyon

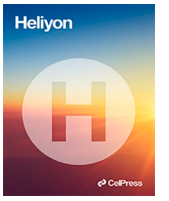

Research article

Novel artemisinin derivative P31 inhibits VEGF-induced corneal neovascularization through AKT and ERK1/2 pathways

Wen Ding [a,b,1], Yingxue Su [a,1], Jianshan Mo [b,1], Danyuan Sun [b], Chen Cao [a], Xiaolei Zhang [b,**], Yandong Wang [a,b,*]

[a] State Key Laboratory of Ophthalmology, Zhongshan Ophthalmic Center, Sun Yat-sen University, Guangdong Engineering Research Center for Ophthalmic Drug Creation and Evaluation, Guangzhou, 510060, China
[b] School of Pharmaceutical Sciences, Sun Yat-Sen University, Guangzhou, 510006, China

A B S T R A C T

Corneal neovascularization (CoNV)is a major cause of blindness in many ocular diseases. Substantial evidence indicates that vascular endothelial growth factor (VEGF) plays an important role in the pathogenesis of corneal neovascularization. Previous evidence showed that artemisinin may inhibit angiogenesis through down regulation of the VEGF receptors. We designed and synthesized artemisinin derivatives, and validated their inhibitory effect on neovascularization in cell and animal models, and explored the mechanisms by which they exert an inhibitory effect on CoNV. Among these derivatives, P31 demonstrated significant anti-angiogenic effects *in vivo* and *in vitro*. Besides, P31 inhibited VEGF-induced HUVECs angiogenesis and neovascularization in rabbit model via AKT and ERK pathways. Moreover, P31 alleviated angiogenic and inflammatory responses in suture rabbit cornea. In conclusion, as a novel artemisinin derivative, P31 attenuates corneal neovascularization and has a promising application in ocular diseases.

1. Introduction

The ocular surface, which includes the cornea, conjunctiva, lacrimal system, and eyelids, is responsible for maintaining a clear refractive surface and protecting the eye from damage and infection [1]. Corneal neovascularization may involve several corneal layers, recent study has shown that the main localization of vascularized corneal buttons is in the upper and mid-third areas of the anterior stroma [2]. Ocular surface neovascularization and its resulting pathological changes significantly alter corneal refraction and obstruct the light path to the retina [3]. Pathologic vessel formation, such as CoNV and abnormal neoplastic vessel formation or peri-limbal vessel loss following chemical or radiation injury, represent significant causes of visual loss [4]. CoNV arises due to a variety of insults including hypoxic injury and ocular surface inflammation due to trauma, infection, chemical burns, and immunological disease [5]. The exact incidence and prevalence of CoNV are unknown, but CoNV is present in many cases of corneal disease, which is the 4th leading cause of blindness globally after cataract, glaucoma and age-related macular degeneration according to the World Health Organization [6].

During the process of vascular neovascularization, neovascularization-promoting factors mainly include VEGF [7], fibroblast growth factor (FGF) [8], angiopoietin (ANG) [9], Hepatocyte growth factor (HGF) [10], platelet-derived growth factor (PDGF),

* Corresponding author. State Key Laboratory of Ophthalmology, Zhongshan Ophthalmic Center, Sun Yat-sen University, Guangdong Engineering Research Center for Ophthalmic Drug Creation and Evaluation, Guangzhou, 510060, China.
** Corresponding author.
E-mail address: wangyd75@mail2.sysu.edu.cn (Y. Wang).
[1] These authors contributed equally to this work.

https://doi.org/10.1016/j.heliyon.2024.e29984
Received 16 January 2024; Received in revised form 18 April 2024; Accepted 18 April 2024
Available online 20 April 2024

transforming growth factor β (TGF-β), matrix-degrading enzymes such as metalloproteinases (MMP), etc. In addition, transcription factors such as hypoxia-inducible factor 1α (HIF-1α) [11], signal transducer and activator of transcription 3 (STAT3), and nuclear transcription factor κB (NF-κB) have been demonstrated to promote vascular neogenesis [12]. VEGF plays the most important role in the pathogenesis of corneal neovascularization [13]. Large molecular weight anti-VEGF protein drugs, including ranibizumab, bevacizumab, aflibercept, and brolucizumab, have revolutionized the treatment of vascular neovascularization [6]. However, incomplete response to anti-VEGF therapy, and specifically persistent disease activity (PDA) and suboptimal vision recovery (SVR), represent significant clinical unmet needs [14].

Artemisinin is an antimalarial drug isolated from Artemisia annua L [15]. There is emerging evidence that artemisinin has multiple pharmacological actions in suppressing inflammation [16], viral infections [17], and tumor proliferation [18]. The derivatives of artemisinin, such as Artesunate [19], dihydroartemisinin [20], arteeter, artemether and artemisone, appear to be more potent than the substance itself [18].

In recent years, its anti-angiogenic effects have attracted much attention. Various models have accumulated mounting evidence, demonstrating the involvement of inhibiting aberrant angiogenesis and corneal neovascularization in the actions of artemisinin and its derivatives [21–24]. Artemisinin reduced the proliferation, migration, and tube formation of HUVEC, as well as the expression of VEGFR1 and VEGFR2 [24]. Similarly, in human umbilical vein endothelial cell (HUVEC) lines, artesunate was shown to inhibit angiogenesis by downregulating the levels of the VEGF receptors [25].

In this study, we evaluated the potential effects and explored mechanisms of a novel artemisinin derivative P31 in the treatment of neovascularization *in vitro* and *in vivo*.

2. Materials and methods

2.1. Animals and ethical statement

New Zealand rabbits were housed at constant temperature (25 °C) with alternating 12 h light–dark cycle and had free access to standard chow and clean water. The animal procedures were approved by the Institutional Animal Care and Use Committee (IACUC), Sun Yat-Sen University (O2021058). The experiments were carried out in compliance with the ARRIVE guidelines (https://arriveguidelines.org) and all methods were performed according to relevant guidelines and regulations.

2.2. Cell lines and cell culture

The human vascular endothelial cell (HUVEC) cell line was from American Type Culture Collection (ATCC, VA, USA), HUVEC cells were cultured in Endothelial Cell Medium (Sciencell, Carlsbad, CA, USA) containing 10 % fetal bovine serum (FBS, Gibco, Carlsbad, CA, USA) and 1 % penicillin-streptomycin (P.S., Gibco, Carlsbad, CA, USA). Cells were incubated in a humidified 5 % CO_2 incubator at 37 °C [26].

2.3. Cell viability and proliferation assay

For the CCK8 assay, cells were seeded into 96-well plates with a density of 10000 cells per well. After 24 h, the cells were treated with 10 ng/ml VEGF (or together with 5uM、25μM and 50uM P31) and cultured in a cell incubator for 24h, 48h and 72 h, then Cell Counting Kit-8 (CCK-8, B34304, Bimake, Houston, TX, USA) was added into a 96-well plate and incubated for 1–4 h at 37 °C. Cell viability was evaluated based on measurements of the optical density at 450 nm using a microplate reader (FLUOstar Omega-ACU, Ortenburg, Germany). The percentage of growth was calculated as Cell viability (%) = [A (Compound +) – A (Blank)]/[A (Compound -) – A (Blank)] × 100 %. Each experiment was done thrice independently.

For EdU (5-Ethynyl-2′-deoxyuridine) assay, cells were seeded into 6-well plates with an appropriate density, after being treated with VEGF (or together with P31) for 3 days in indicated concentrations, the EdU assay was performed according to the manufacturer's protocol of BeyoClickTMEdU-555 Cell Proliferation Kit (C0075S, Beyotime, Shanghai, China). Cells were treated with the corresponding concentration of EdU reagent for 2 h in a cell incubator at 37 °C, 5 % CO2, then discarded culture medium and added into 4 % paraformaldehyde for fixation at room temperature for 15 min. After washing with PBS containing 3 % BSA for 5 min twice, cells were permeated with 0.3 % TritonX-100 for 15 min at room temperature. After permeating, the cells were washed twice and dyed with EdU reaction solution to indicate proliferation. A fluorescence microscope was used to capture the image [27].

2.4. Scratch wound healing assay

HUVECs were seeded onto 6-well tissue culture plates and were cultured for 24 h as a monolayer (100 % confluence). A sterile pipette tip was used to make a scratch in the monolayer perpendicularly across the center of the well. The floating cells were washed away with warm PBS. HUVECs were treated with VEGF (or together with P31). Images were taken at 0 and 12 h after wounding with a Microscope. Mitomycin (1.0 μg/ml; Sigma-Aldrich) was always added to exclude the influence of cell proliferation [28]. Each experiment with triplicate samples was continuously performed 3 times, and the percentage of recovery was calculated according to the following formula: recovery (%) = $(S_0 - S_{12}/S_0) \times 100$ %. S_0 represents the area of the original blank area, and S_{12} represents the area of the blank area after 12 h.

2.5. Transwell migration array

Transwell chambers with 8 μm pore filters (Corning, Corning, NY, USA) were precoated with 1 mg/ml Matrigel (BD Biosciences, San Jose, CA, USA). HUVEC (5×10^4 cells of each chamber) were starved overnight and added to the upper chamber, and the lower chamber was filled with complete medium with VEGF (or together with P31). After 24 h, cells were immersed into 3 % para-formaldehyde for 15 min, stained with crystal violet, and counted under a light microscope [29].

2.6. Tube formation assay

HUVECs (1×10^3 cells per well) were seeded onto 96-well tissue culture plates precoated with basement membrane matrix (BD Biosciences). Cells were then treated with VEGF (or together with P31) for 4 h. The tube formation was photographed under an Olympus Microscope [28].

2.7. Western blot and immunoprecipitation

Cells were lysed with RIPA lysis buffer (Beyotime, Shanghai, China) supplemented with protease inhibitors (Beyotime, Shanghai, China) and phosphatase inhibitors cocktail (Bimake, Houston, TX, USA) after being treated with the indicated concentrations of the drug. Whole cell lysates were measured using a BCA Protein Assay Kit (Thermo Fisher, Waltham, MA, USA) and denatured for 5 min by heating in 99 °C. The protein samples were electrophoresed through a 5 %~12 % SDS-PAGE gel and transferred to polyvinylidene fluoride (PVDF) membranes (Merck Millipore, Darmstadt, Germany). Membranes were blocked and probed by indicated primary antibodies: anti-AKT (ABclonal)、anti-AKT1/2 (ABclonal)、anti-ERK (ABclonal)、anti-ERK1/2 (ABclonal)、anti-GAPDH (Servicebio), as the manufacturer's instructions and followed by the appropriate anti-mouse/rabbit horseradish peroxidase (HRP)-conjugated secondary antibody. After that, the membranes were imaged by a chemiluminescence instrument (Bio-Rad, Hercules, CA, USA).

2.8. RNA extraction and quantitative real-time PCR

Total cellular RNA was extracted by using Trizol (YEASEN, Shanghai, China) according to the manufacturer's protocol and cDNAs were obtained from 2 μg total RNA reverse-transcription by using Hifair® II 1st Strand cDNA Synthesis Kit (YEASEN, Shanghai, China) according to the manufacturer's protocol. Quantitative real-time PCR (QPCR) analyses were conducted by a CFX Connect™ real-time system (Bio-Rad, Hercules, CA, USA) with SYBR Green master mix (YEASEN, Shanghai, China). The specific primers were used to detect mRNA expression levels of VEGF, VEGFR, PDGF-β, MMP-9, VACM-A, ANG-1, NOS-1, IL-1, IL-6, TNF-α, PEDF and CD144, and β-Actin expression levels were used for normalization [30](Table 1).

Table 1
The sequences of related genes in ChIP-qPCR analysis.

Gene	Primer squence
VEGF promoter	F:5′-TGCGGATCAAACCTCACCAA-3′ R: 5′-GGCTCCAGGGCATTAGACAG-3′
VEGFR promoter	F:5′-CGGTCAACAAAGTCGGGAGA-3′ R: 5′-CAGTGCACCACAAAGACACG-3′
PDGF-βpromoter	F:5′-GCCAGCGCCCATTTTTCATT-3′ R: 5′-TTTCTCTTTGCAGCGAGGCT-3′
MMP-9 promoter	F:5′-TCTATGGTCCTCGCCCTGAA-3′ R: 5′-CATCGTCCACCGGACTCAAA-3′
VACM-A promoter	F:5′-GGACCACATCTACGCTGACA-3′ R: 5′-TTGACTGTGATCGGCTTCCC-3′
ANG-1 promoter	F:5′-GCTGAACGGTCACACAGAGA-3′ R: 5′-GTACTGCCAGCACACTCCTT-3′
NOS-1 promoter	F:5′-CAAACACGCCTTTGATGCCA-3′ R: 5′-CAAGGGTTCCGGGTACTTCC-3′
IL-1 promoter	F:5′-AACCTCTTCGAGGCACAAGG-3′ R: 5′-AGCCATCATTTCACTGGCGA-3′
IL-6 promoter	F:5′-TTCGGTCCAGTTGCCTTCTC-3′ R: 5′-TGTTTTCTGCCAGTGCCTCT-3′
TNF-αpromoter	F:5′-TCTTCTCGAACCCCGAGTGA-3′ R: 5′-TATCTCTCAGCTCCACGCCA-3′
PEDF promoter	F:5′-GTGCAGGCTTAGAGGGACT-3′ R: 5′-AGGAGGGCTCCAATGCAGA-3′
CD144 promoter	F:5′-CCCACAGGCACGATCTGTT-3′ R: 5′-CATTCTTGCGACTCACGCTT-3′
β-Actin promoter	F:5′-ACTCTTCCAGCCTTCCTTCC-3′ R: 5′-CGTACAGGTCTTTGCGGATG-3′

2.9. In vivo studies

A total of 15 New Zealand rabbits were used. the animals were divided into a control group and two concentration dosing groups. New Zealand rabbits were intramuscularly injected with SU-MIAN-XIN at a dose of 0.35 ml/kg. Tobramycin eye drops were used to rinse the conjunctival sac, and surface anesthesia with procaine was performed twice before surgery. After anesthesia, a speculum was used to open the eyelid. The suture was located 3.0 mm inside the corneal limbus at the 12:00 o'clock position, and a 10 0 nylon double loop radial suture was used. The suture span was about 3 mm, reaching a depth of 1/2-2/3 corneal thickness. The length of the suture head was about 1 mm, and the distance between the radial suture lines was about 1 mm. P31 was given three times a day in the P31 treated group and PBS was given three times a day in the control group. 5 New Zealand rabbits per group. On the third day after surgery, ofloxacin eye drops were used to resist infection in the surgical eyes. On the 1, 7 and 15 days after medication, photos were taken using a slit lamp (BX-900, Haag Streit Gruppe, CH) to observe the presence of corneal sutures and the growth trend of CoNV in rabbits. The branches of vessels were determined by ImageJ software (Image Processing and Analysis in Java; National Institutes of Health, Bethesda, MD, USA; https://imagej.nih.gov/ij/).

2.10. Statistical analysis

Statistical analysis was performed on mean values using Prism (GraphPad Software, USA). The significance of differences between groups was determined via the unpaired *t*-test as *P < 0.05, **P < 0.01, ***P < 0.001.

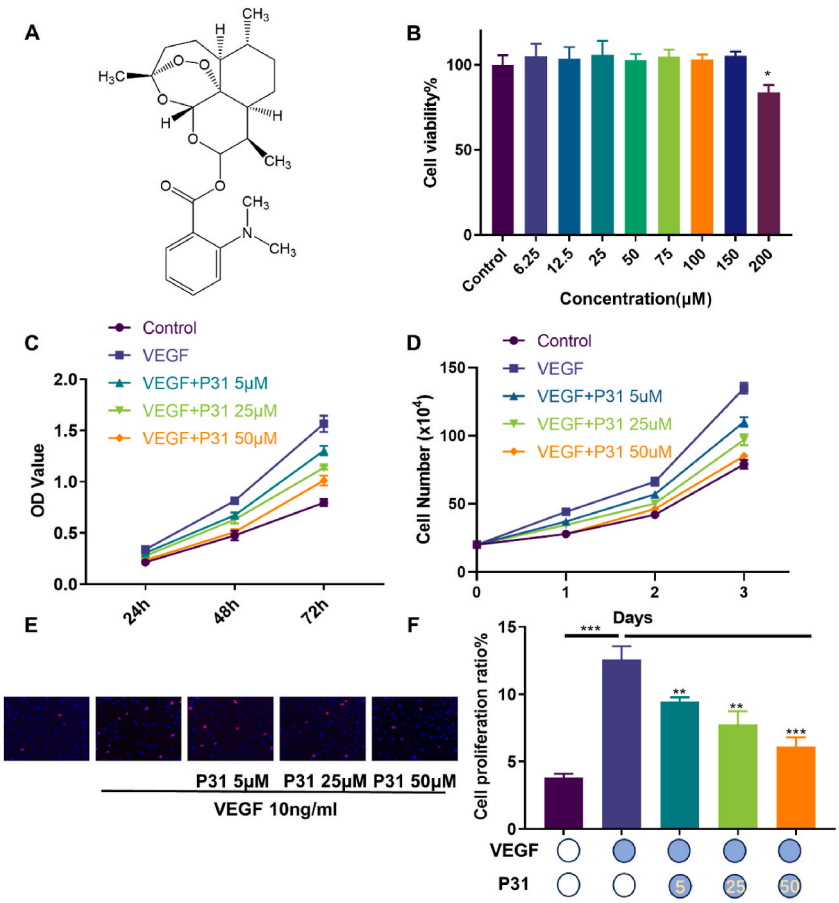

Fig. 1. |P31 inhibited VEGF-induced proliferation of HUVECs. (A) Chemical structure of artemisinin derivatives. (B) The effect of different concentrations of P31 on HUVECs toxicity in CCK8 assay. (C) VEGF induced HUVECs cells were treated with 5, 25 and 50 μM P31 for 24, 48 and 72 h, and cell viability was measured by CCK-8 assay. (D) p31 reduced the number of cells in VEGF induced HUVECs proliferation. (E, F) HUVECs proliferation induced by VEGF without or with treatment with P31 was determined using BrdU assays. All data are shown as the mean ± SEM from three independent experiments. *P < 0.05, **P < 0.01, ***P < 0.001.

3. Result

3.1. P31 inhibited VEGF-induced proliferation of HUVECs

P31 was selected from dozens of artemisinin derivatives, and its structure is shown in Fig. 1A. Firstly, we detected the safety of P31 using CCK-8 assay. P31 did not exhibit cytotoxic effect on HUVECs at up to 150 μM. Limited cytotoxicity was observed at 200 μM. (Fig. 1 B).We further investigated whether P31 exerts anti-proliferative effect on HUVECs after VEGF induction. After HUVECs were stimulated with VEGF, cells were treated with different concentrations of P31 for 4 h, and cell number was measured through CCK-8 assay (Fig. 1C and D).VEGF stimulation resulted in increased HUVECs proliferation, whereas P31 attenuated the VEGF-induced cell proliferation in a dose-dependent manner. BrdU staining confirmed that P31 suppressed VEGF-induced HUVECs proliferation (Fig. 1 E, F).

3.2. P31 inhibits VEGF-induced HUVECs migration, invasion

Cell migration and invasion are essential to angiogenesis. Since we observed the anti-angiogenesis properties of P31, we further investigated its effect on VEGF-induced HUVECs migration and invasion. As shown in Fig. 2A, VEGF treatment promotes cell invasion of HUVECs compared to the control group ($p < 0.01$) (Fig. 2 A, B). While P31 significantly inhibited the invasion of HUVECs in a dose-dependent manner ($p < 0.01$). The treatment of cells with increasing concentration of P31 caused a concentration-dependent decrease in wound-healing cell migration (Fig. 2C, D).

3.3. P31 inhibited VEGF-induced HUVECs angiogenesis via AKT and ERK1/2 pathways

The formation of tube-like vessels is a classical approach to assess the effect of candidate compound on angiogenesis. VEGF stimulation resulted in a rich network of branched capillary-like tubes after HUVECs seeding on Matrigel (Fig. 3A–C). In the presence of P31 (5, 25, 50 μM), tube formation was interrupted on VEGF-treated HUVECs with a capillary length dropping to 21.64 %、25.64 %、35.8 % respectively, a total branch points dropping to 23.62 %、36.22 % and 43.3 %. These data indicated that P31 suppressed angiogenesis of endothelial cells in the presence of VEGF. Since activation of VEGF pathway plays a key role in angiogenesis, we investigated whether P31 supresses angiogenesis by inhibiting the activation of AKT and ERK1/2 signaling pathways. Anti-angiogenic effect of P31 in VEGF-induced HUVECs was further investigated using Western blot and RT-qPCR. The levels of phosphorylation of ERK1/2 and AKT were examined in comparison with the control ($p < 0.05$), whereas the total expression of ERK1/2 and AKT did not change significantly after P31 treatment (Fig. 3D). VEGF significantly increased the mRNA levels of CD144、MMP-9 and PDGF-β in cultured HUVECs, whereas treatment of P31 decreased the mRNA levels of CD144、MMP-9 and PDGF-β (Fig. 3E). These data showed that P31 inhibited AKT and ERK1/2 signaling of VEGF-induced HUVECs *in vitro*.

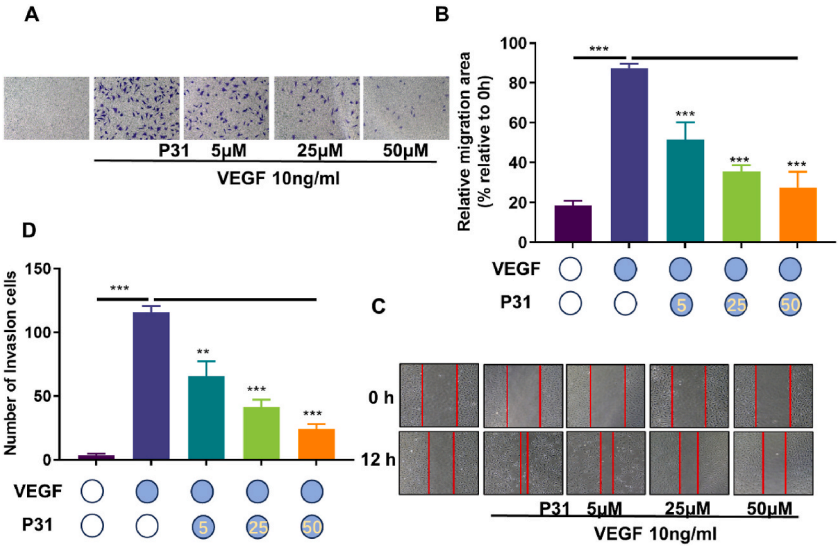

Fig. 2. |P31 inhibits VEGF-induced HUVECs migration, invasion. (A, B) P31 inhibited VEGF-induced invasion of HUVECs in transwell assay. (C, D) P31 inhibited VEGF-induced migration of HUVECs in the cell scratch test. All data are shown as the mean ± SEM from three independent experiments. *P < 0.05, **P < 0.01, ***P < 0.001.

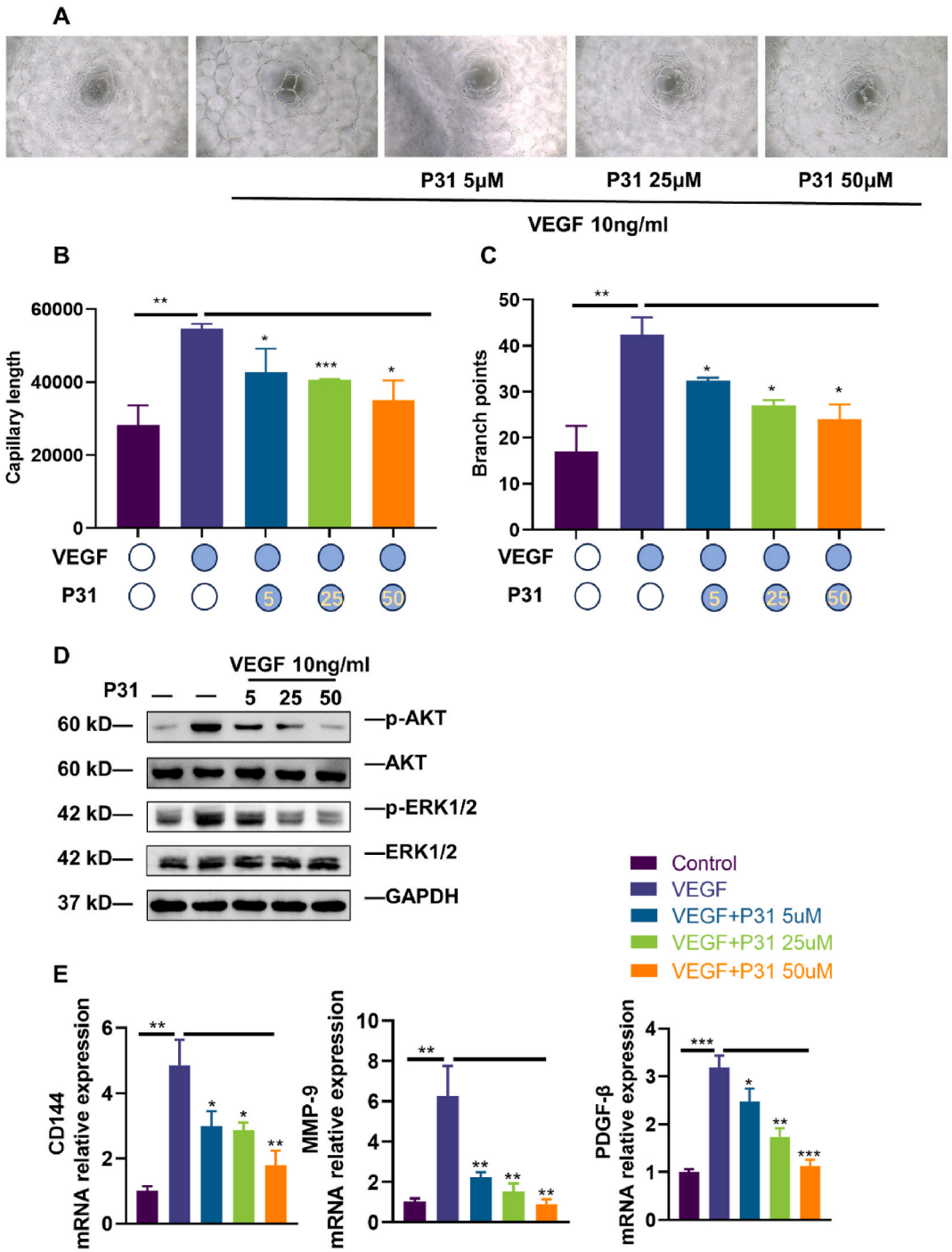

Fig. 3. |P31 inhibited VEGF-induced HUVECs angiogenesis via AKT and ERK pathways. (A–C) HUVECs plated on Matrigel-coated plates were treated with VEGF in the presence or absence of P31. After 4 h, tube formation was photographed, tube length and branch points were quantitated using Image-Pro Plus software. (D) VEGF-induced HUVECs treated with P31 (5, 25 and 50 μM), the phosphorylation levels of AKT and ERK pathway were analyzed by Western blot. (E) The mRNA expression of CD144, MMP-9 and PDGF-β in VEGF-induced HUVECs were treated with P31 (5, 25 and 50 μM) by RT-qPCR. All data are shown as the mean ± SEM from three independent experiments. *P < 0.05, **P < 0.01, ***P < 0.001.

3.4. P31 attenuates retinal neovascularization in rabbit models

The animal studies were divided into three groups, the control group, the 1 % P31 group and the 2 % P31 group.As shown in the images from slit lamp microscopy, we found that P31 reduced the length and new blood vessel area of corneal NV compared with the

control group (Fig. 4A–C). Hematoxylin and eosin (H&E) staining further showed that P31 significantly inhibited corneal neovascularization (black arrows) compared to the control group (Fig. 4 D).

We further examined the protein levels of the VEGF-related factors ERK1/2 and AKT in rabbit corneal tissue. Our results showed that the AKT and ERK1/2 signaling pathway was inhibited by P31, indicated by down regulation of phosphorylation of AKT and ERR1/2 in VEGF-induced HUVECs cell and rabbit model (Fig. 4 E).

3.5. P31 alleviated angiogenic and inflammatory responses in suture-induced corneal neovascularization rabbit model

Upregulation of key proinflammatory cytokines, including interleukin-1 (IL-1), interleukin-6 (IL-6), tumor necrosis factor (TNF-α) and Nitric oxide synthase 1 (NOS-1) [31,32], as well as the proangiogenic molecules VEGF, matrix metalloproteinase 9 (MPP-9), Platelet derived growth factor-β (PDGF-β), Vascular 57 cell adhesion molecule-1 (VCAM-1), Angiopoietin-1 (ANG-1) and VE-cadherin (CD144),as well as vascular endothelial growth factor receptor (VEGFR) [33], is critically involved in pathogenesis of CoNV. Conversely, pigment epithelium-derived factor (PEDF) is an antiangiogenic molecule [34].Results showed that the mRNA expression of VEGF (Fig. 5 A), VEGFR (Fig. 5 B), PDGF-β (Fig. 5C), VCAM-1 (Fig. 5 D), MPP-9 (Fig. 5 E), ANG-1 (Fig. 5 F), NOS-1 (Fig. 5 G), IL-1 (Fig. 5H), IL-6 (Fig. 5 I), TNF-a (Fig. 5 J) and CD144 (Fig. 5 L) were significantly increased in the vascularized area of Suture damaged cornea. Conversely, expression of PEDF (Fig. 5 K) mRNA was decreased. While treatment of P31 eyedrops significantly down regulated suture damage–induced expression changes of these cytokines. Thus, P31 alleviated angiogenic and inflammatory responses in alkali-burned rabbit cornea.

4. Discussion

The cornea, which is the primary refractive surface of the anterior part of the eye, is essential for having the best possible vision [35]. For more than 1.4 million people each year, corneal neovascularization (CoNV) is a disorder that threatens their ability to see. It may cause tissue scarring, edema, lipid buildup, and ongoing inflammation, which may hurt quality of life and visual prognosis [36]. The therapeutical strategies of CoNV consist of off-label use of anti-VEGF antibodies, such as bevacizumab [37]. Bevacizumab showed encouraging results in the treatment of CoNV, but its usage has been constrained by partial efficacy, resistance, and adverse effects including corneal thinning and impaired epithelial repair. Therefore, the need for safer and better treatments for CoNV is critical [38].

Artemisinin (ART) is a bioactive molecule derived from the Chinese medicinal plant Artemisia annua (Asteraceae). Artemisinin is renowned for its recognized anti-malaria activity, and recent studies have shown that it can also promote apoptosis [39], inhibit inflammation [40], and have anti-angiogenic [41] effects. In animal models, Cheng et al. [42] demonstrated that artesunate could inhibit CoNV by inducing ROS-dependent apoptosis. Geng et al. [43], suggest that Artesunate inhibits choroidal melanoma

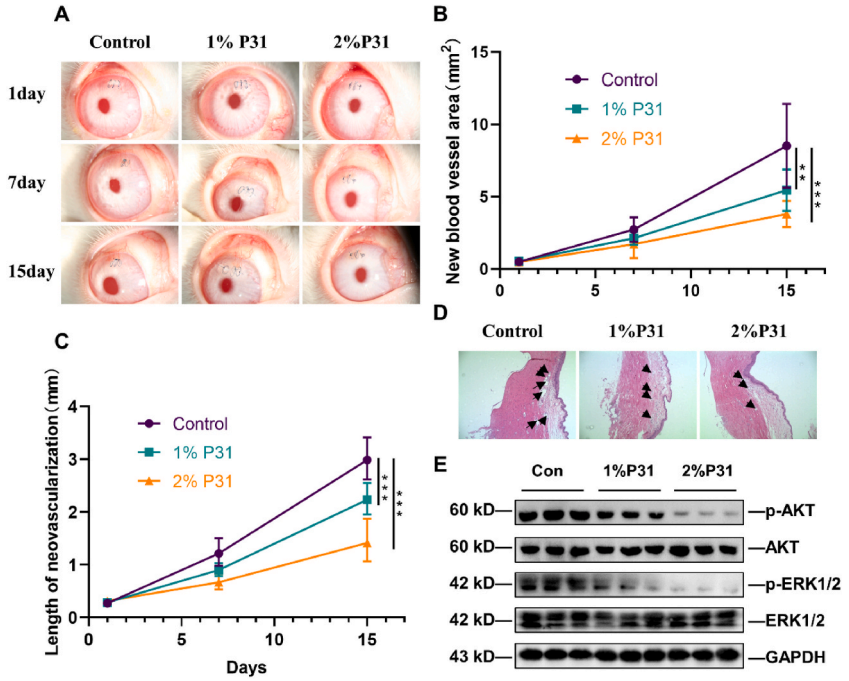

Fig. 4. |P31 inhibited neovascularization in rabbit model by AKT and ERK1/2 pathways. (A) Effect of P31 on suture-induced corneal NV status by slit lamp microscopy (n = 5). (B,C) Length,new blood vessel area of corneal NV at 1,7 and 15 days after suturing (n = 5). (D) H&E staining of cross-sections of the cornea of rabbit (n = 3). (E) Western blot analysis of AKT, ERK1/2, *p*-AKT, and *p*-ERK1/2 expression levels in rabbit corneal tissue treated with P31 (n = 3). All data are shown as the mean ± SEM from three independent experiments. *P < 0.05, **P < 0.01, ***P < 0.001.

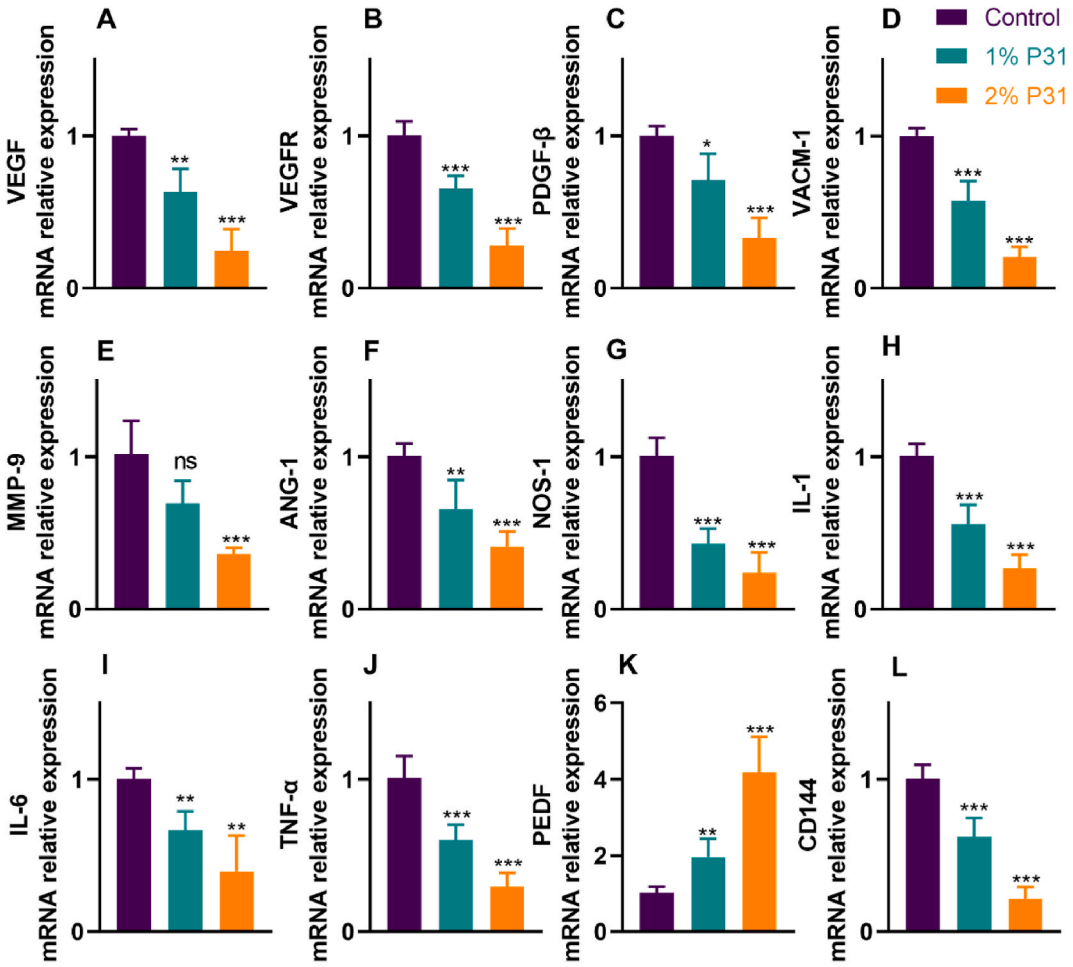

Fig. 5. |P31 inhibits suture–induced mRNAs change in Rabbit cornea. Total mRNA was isolated from vascularized areas of cornea with Suture damage, with 1 % P31 or 2 % P31 or without P31 eyedrops (n = 3). Relative expression of VEGF mRNA (A), VEGFR mRNA (B), PDGF-β mRNA (C), MMP-9 mRNA (D), VACM-1 mRNA (E), ANG-1 mRNA F), NOS-1 mRNA (G), IL-1 mRNA (H), IL-6 mRNA (I), TNF-α mRNA (J), PEDF mRNA (K), and CD144 mRNA (L). β-Actin mRNA was detected as internal control. All data are shown as the mean ± SEM from three independent experiments. *P < 0.05, **P < 0.01, ***P < 0.001.

angiogenesis via the Wnt/CaMKII signaling axis.

The shortcomings of ART include a short plasma half-life, limited bioavailability, and poor solubility in oil and water [44]. P31 has more polar groups in its chemical structure than artemisinin. It has suitable solubility and is relatively stable under storage conditions. Pharmacogenetic experiments have shown that P31 can be detected in ocular tissues and is distributed in the cornea, conjunctiva, and aqueous humor to achieve a high concentration of the drug, making it an excellent artemisinin precursor drug. Here, we reported that an ARS-type compound P31 exhibits significant antiangiogenic activity *in vitro* and *in vivo* by inhibiting injury-induced rises in VEGF. Firstly, we used the CCK-8 assay to detect the toxicity of P31, we found that P31 is essentially non-toxic to cells, which suggests that P31 is a promising anti-angiogenic agent. VEGF was demonstrated to play the most important role in promoting endothelial cell mitogenesis and retinal vessel permeability [7], we found that P31 notably inhibited VEGF-induced proliferation、migration、invasion and tube formation of vascular endothelial cells of HUVECs. These experiments allowed us to directly observe the anti-angiogenesis of P31 *in vitro*. Angiogenesis is a complex process, composed of dissociations of pericytes from the preexisting vessel, digestion of extracellular matrix with protease growth, migration, invasion, tube formation [45,46].

A great number of pro-angiogenic factors, such as TNF-α, ANG-1 and MMPs, mediate angiogenesis in diseases [31,32]. CD144 (VE-Cadherin) is an adhesion protein expressed in endothelial cells, belongs to the cadherin family of transmembrane proteins. Genes in association with angiogenesis and vasculogenesis are upregulated in aggressive cancer cells that contribute to glioma formation [47,48]. The expression of MMP-9 may influence the balance between angiogenic and antiangiogenic factors [49]. Vascular endothelial growth factor (VEGF) is a member of the vascular endothelial growth factor family, which promotes the proliferation and migration of endothelial cells and plays a vital role in vascular growth, maturation, stabilization and remodeling [34].We found that P31 downregulated the mRNA expression of CD144、MMP-9 and PDGF-β in VEGF-induced HUVECs. In addition, P31 also inhibited angiogenesis by downregulating VEGF, TNF-α, IL-1, PDGF, and TGF-β in the rabbit model.

We used the suture method to construct a rabbit model of corneal neovascularization. All model rabbits began to gradually close their eyes with lid conjunctival congestion on the first day after surgery. The cornea gradually started to diffusely edematize and produce new blood vessels. This inflammatory response may be related to the reduced oxygen supply to the corneal surface due to sutures acting as a traumatic foreign body with compensatory dysregulation. Slit-lamp images show the successful modeling and the anti-angiogenic effect of P31.

The mechanism of anti-VEGF drugs for the treatment of CoNV still needs to be further explored [14]. VEGF-mediated pro-angiogenesis signaling acts through PI3K/Akt-dependent signaling pathway [50] and MEK1/2/ERK1/2 pathway [51]. Our results show that the AKT and ERK1/2 signaling pathway was blocked by down regulating their phosphorylation in VEGF-induced HUVECs and rabbit model treated with P31.

VEGF is a major target of anti-angiogenesis, but recently many new anti-angiogenic targets have emerged. Novel molecular targets, such as TGF-β [52], angiopoietins [33], AKT, ERK1/2, and their receptors, as well as other hypoxia-regulated gene products also provide avenues for improving the therapeutic benefit of anti-NV strategies. Our results prove that P31 can cover VEGF, AKT, and ERK1/2 targets, with great penetrability and durable efficacy and may partially solve the issue of the limited efficacy of and resistance to anti-VEGF therapy alone.

Our results provide initial evidence that P31 has a good ability to inhibit the proliferation, migration, and tube formation of HUVECs. Furthermore, the AKT and ERK1/2 signaling pathway was blocked by down regulating their phosphorylation in VEGF-induced HUVECs and rabbit model treated with P31. In summary, P31 demonstrated a significantly anti-angiogenic effect *in vivo* and *in vitro*. Besides, P31 inhibited VEGF-induced HUVECs angiogenesis and neovascularization in rabbit model via AKT and ERK pathways. Moreover, P31 alleviated angiogenic and inflammatory responses in a suture-induced corneal neovascularization rabbit model. The present study might provide support and evidence for the application of derivatives of artemisinin in the clinical treatment of conditions related to ocular diseases.

Data availability statement

[1] PMID: 35328532 [11]. PMID: 34128478 [24]. PMID: 36321394 [27]. PMID: 36849939 [31]. PMID: 36537293 [39]. PMID: 32647692 [40]. PMID: 33138094.

CRediT authorship contribution statement

Wen Ding: Writing – review & editing, Writing – original draft, Visualization, Validation, Software, Resources, Methodology, Investigation, Data curation, Conceptualization. **Yingxue Su:** Writing – original draft, Visualization, Software, Resources, Project administration, Funding acquisition, Data curation, Conceptualization. **Jianshan Mo:** Writing – original draft, Visualization, Supervision, Software, Formal analysis, Data curation. **Danyuan Sun:** Visualization, Methodology, Funding acquisition, Data curation. **Chen Cao:** Writing – original draft, Software, Project administration. **Xiaolei Zhang:** Writing – review & editing, Writing – original draft, Funding acquisition, Formal analysis. **Yandong Wang:** Writing – review & editing, Writing – original draft, Supervision, Funding acquisition.

Declaration of competing interest

The authors declare that they have no known competing financial interests or personal relationships that could have appeared to influence the work reported in this paper.

Acknowledgments

This work was supported by the National Natural Science Foundation of China (81500739), Natural Science Foundation of Guangdong Province (2023A1515012521), Traditional Chinese Medicine Bureau of Guangdong Province (20231079), and Science and Technology Program of Guangzhou (202103000050).

Appendix A. Supplementary data

Supplementary data to this article can be found online at https://doi.org/10.1016/j.heliyon.2024.e29984.

References

[1] D'Souza Das, Gorimanipalli, et al., Ocular surface infection mediated molecular stress responses: a review [J], Int. J. Mol. Sci. 23 (6) (2022).
[2] Kempuraj Mohan, D'Souza, et al., Corneal stromal repair and regeneration [J], Prog. Retin. Eye Res. 91 (2022) 101090.
[3] ZhongCui Yang, et al., Up-to-date molecular medicine strategies for management of ocular surface neovascularization [J], Adv. Drug Deliv. Rev. 201 (2023) 115084.
[4] SunCui Yu, et al., Three kinds of corneal host cells contribute differently to corneal neovascularization [J], EBioMedicine 44 (2019) 542–553.

[5] Kolko Baudouin, Melik Parsadaniantz, et al., Inflammation in Glaucoma: from the back to the front of the eye, and beyond [J], Prog. Retin. Eye Res. 83 (2021) 100916.
[6] Langer Cao, Ferrara. Targeting angiogenesis in oncology, ophthalmology and beyond [J], Nat. Rev. Drug Discov. 22 (6) (2023) 476–495.
[7] Chen Apte, Ferrara. VEGF in signaling and disease: beyond discovery and development [J], Cell 176 (6) (2019) 1248–1264.
[8] Katoh, Therapeutics targeting FGF signaling network in human diseases [J], Trends Pharmacol. Sci. 37 (12) (2016) 1081–1096.
[9] LuckSchering Felcht, et al., Angiopoietin-2 differentially regulates angiogenesis through TIE2 and integrin signaling [J], J. Clin. Invest. 122 (6) (2012) 1991–2005.
[10] SuriAmouzegar Omoto, et al., Hepatocyte growth factor suppresses inflammation and promotes epithelium repair in corneal injury [J], Mol. Ther. 25 (8) (2017) 1881–1888.
[11] QinMartinez Zhang, et al., HIF-1α and HIF-2α redundantly promote retinal neovascularization in patients with ischemic retinal disease [J], J. Clin. Invest. 131 (12) (2021).
[12] ZhangLu Tang, et al., Melatonin maintains inner blood-retinal barrier by regulating microglia via inhibition of PI3K/Akt/Stat3/NF-κB signaling pathways in experimental diabetic retinopathy [J], Front. Immunol. 13 (2022) 831660.
[13] ChenZheng Liu, et al., Angiogenic signaling pathways and anti-angiogenic therapy for cancer [J], Signal Transduct. Targeted Ther. 8 (1) (2023) 198.
[14] Allingham Mettu, Cousins. Incomplete response to Anti-VEGF therapy in neovascular AMD: exploring disease mechanisms and therapeutic opportunities [J], Prog. Retin. Eye Res. 82 (2021) 100906.
[15] ZhangLiao Ma, et al., The birth of artemisinin [J], Pharmacol. Ther. 216 (2020) 107658.
[16] Zeng Huai, Ge, Artemisinin ameliorates intestinal inflammation by skewing macrophages to the M2 phenotype and inhibiting epithelial-mesenchymal transition [J], Int. Immunopharm. 91 (2021) 107284.
[17] CaoQiu Feng, et al., Traditional application and modern pharmacological research of Artemisia annua L [J], Pharmacol. Ther. 216 (2020) 107650.
[18] Efferth, From ancient herb to modern drug: Artemisia annua and artemisinin for cancer therapy [J], Semin. Cancer Biol. 46 (2017) 65–83.
[19] PanTong Liu, et al., Artesunate protects against ocular fibrosis by suppressing fibroblast activation and inducing mitochondria-dependent ferroptosis [J], Faseb. J. 37 (6) (2023) e22954.
[20] ZhangChen Dai, et al., Dihydroartemisinin: a potential natural anticancer drug [J], Int. J. Biol. Sci. 17 (2) (2021) 603–622.
[21] LiLi Yuan, et al., Artemisinin, a potential option to inhibit inflammation and angiogenesis in rosacea [J], Biomed. Pharmacother. 117 (2019) 109181.
[22] HeWang Bao, et al., Artemisinin and its derivate alleviate pulmonary hypertension and vasoconstriction in rodent models [J], Oxid. Med. Cell. Longev. 2022 (2022) 2782429.
[23] HuangHan Wang, et al., The effects of artemisinin on the proliferation and apoptosis of vascular smooth muscle cells of rats [J], Cell Biochem. Funct. 32 (2) (2014) 201–208.
[24] XiangHua Yu, et al., Artemisinin suppressed tumour growth and induced vascular normalisation in oral squamous cell carcinoma via inhibition of macrophage migration inhibitory factor [J], Oral Dis. 30 (2) (2024) 363–375.
[25] ZhouWu Chen, et al., Inhibitory effects of artesunate on angiogenesis and on expressions of vascular endothelial growth factor and VEGF receptor KDR/flk-1 [J], Pharmacology 71 (1) (2004) 1–9.
[26] JiangZhao Shan, et al., SCF/c-Kit-activated signaling and angiogenesis require Gαi1 and Gαi3 [J], Int. J. Biol. Sci. 19 (6) (2023) 1910–1924.
[27] DengPeng Mo, et al., Targeting STAT3-VISTA axis to suppress tumor aggression and burden in acute myeloid leukemia [J], J. Hematol. Oncol. 16 (1) (2023) 15.
[28] LiYu Zhang, et al., Ginsenoside Rh2 inhibits vascular endothelial growth factor-induced corneal neovascularization [J], Faseb. J. 32 (7) (2018) 3782–3791.
[29] SiChen Lv, et al., TBX2 over-expression promotes nasopharyngeal cancer cell proliferation and invasion [J], Oncotarget 8 (32) (2017) 52699–52707.
[30] LiLou Ouyang, et al., Inhibition of STAT3-ferroptosis negative regulatory axis suppresses tumor growth and alleviates chemoresistance in gastric cancer [J], Redox Biol. 52 (2022) 102317.
[31] YerneniAzambuja Ludwig, et al., TGFβ(+) small extracellular vesicles from head and neck squamous cell carcinoma cells reprogram macrophages towards a pro-angiogenic phenotype [J], J. Extracell. Vesicles 11 (12) (2022) e12294.
[32] LiYin Zhang, et al., Monocytes deposit migrasomes to promote embryonic angiogenesis [J], Nat. Cell Biol. 24 (12) (2022) 1726–1738.
[33] ChaiLiu Liu, et al., Osteoclasts protect bone blood vessels against senescence through the angiogenin/plexin-B2 axis [J], Nat. Commun. 12 (1) (2021) 1832.
[34] ZhaoZang Du, et al., Artemisinin attenuates the development of atherosclerotic lesions by the regulation of vascular smooth muscle cell phenotype switching [J], Life Sci. 237 (2019) 116943.
[35] Mysore Nicholas, Corneal neovascularization [J], Exp. Eye Res. 202 (2021) 108363.
[36] Park Barry, Corson. Pharmacological potential of small molecules for treating corneal neovascularization [J], Molecules 25 (15) (2020).
[37] McSoleyAmparo Dohlman, et al., Bevacizumab in high-risk corneal transplantation: a pilot multicenter prospective randomized control trial [J], Ophthalmology 129 (8) (2022) 865–879.
[38] AltintasAltintas Ozdemir, et al., Comparison of the effects of subconjunctival and topical anti-VEGF therapy (bevacizumab) on experimental corneal neovascularization [J], Arq. Bras. Oftalmol. 77 (4) (2014) 209–213.
[39] GanHan Chen, et al., Artesunate induces apoptosis and inhibits the proliferation, stemness, and tumorigenesis of leukemia [J], Ann. Transl. Med. 8 (12) (2020) 767.
[40] Hur Lee, Sung, The effect of artemisinin on inflammation-associated lymphangiogenesis in experimental acute colitis [J], Int. J. Mol. Sci. 21 (21) (2020) 8068.
[41] SongLim Jeong, et al., Repurposing the anti-malarial drug artesunate as a novel therapeutic agent for metastatic renal cell carcinoma due to its attenuation of tumor growth, metastasis, and angiogenesis [J], Oncotarget 6 (32) (2015) 33046–33064.
[42] LiLi Cheng, et al., The artemisinin derivative artesunate inhibits corneal neovascularization by inducing ROS-dependent apoptosis in vascular endothelial cells [J], Invest. Ophthalmol. Vis. Sci. 54 (5) (2013) 3400–3409.
[43] ZhuYuan Geng, et al., Artesunate suppresses choroidal melanoma vasculogenic mimicry formation and angiogenesis via the wnt/CaMKII signaling Axis [J], Front. Oncol. 11 (2021) 714646.
[44] XiaWang Shi, et al., Discovery and repurposing of artemisinin [J], Front. Med. 16 (1) (2022) 1–9.
[45] XuZhong Jiang, et al., Research progress of VEGFR small molecule inhibitors in ocular neovascular diseases [J], Eur. J. Med. Chem. 257 (2023) 115535.
[46] KloepperAmoozgar Fukumura, et al., Enhancing cancer immunotherapy using antiangiogenics: opportunities and challenges [J], Nat. Rev. Clin. Oncol. 15 (5) (2018) 325–340.
[47] Qin Li, Elevated circulating VE-cadherin+CD144+endothelial microparticles in ischemic cerebrovascular disease [J], Thromb. Res. 135 (2) (2015) 375–381.
[48] LiYang Liu, et al., IGFBP2 promotes vasculogenic mimicry formation via regulating CD144 and MMP2 expression in glioma [J], Oncogene 38 (11) (2019) 1815–1831.
[49] WangHe Zhang, et al., Regulation of matrix metalloproteinases 2 and 9 in corneal neovascularization [J], Chem. Biol. Drug Des. 95 (5) (2020) 485–492.
[50] LiZhang Xiong, et al., PRL-3 promotes the peritoneal metastasis of gastric cancer through the PI3K/Akt signaling pathway by regulating PTEN [J], Oncol. Rep. 36 (4) (2016) 1819–1828.
[51] Maldonado Estrada, Mallipattu. Therapeutic inhibition of VEGF signaling and associated nephrotoxicities [J], J. Am. Soc. Nephrol. 30 (2) (2019) 187–200.
[52] Pein Hongu, Insua Rodríguez, et al., Perivascular tenascin C triggers sequential activation of macrophages and endothelial cells to generate a pro-metastatic vascular niche in the lungs [J], Nat Cancer 3 (4) (2022) 486–504.